Ultramicroscopy 156 (2015) 50–58

Contents lists available at ScienceDirect

Ultramicroscopy

journal homepage: www.elsevier.com/locate/ultramic

Element-specific Kikuchi patterns of Rutile

M. Vos [a,*], A. Winkelmann [b], G. Nolze [c]

[a] Atomic and Molecular Physics Laboratories, Research School of Physics and Engineering, The Australian National University, Canberra, 0200, Australia
[b] Bruker Nano GmbH, Am Studio 2D, Berlin, Germany
[c] Federal Institute for Materials Research and Testing, Unter den Eichen 87, 12205 Berlin, Germany

ARTICLE INFO

Article history:
Received 21 December 2014
Received in revised form
23 April 2015
Accepted 26 April 2015
Available online 28 April 2015

Keywords:
Electron Rutherford backscattering
TiO_2
Kikuchi pattern
Simulation

ABSTRACT

The kinetic energy of keV electrons backscattered from a rutile (TiO_2) surface depends measurably on the mass of the scattering atom. This makes it possible to determine separately the angular distribution of electrons backscattered elastically from either Ti or O. Diffraction effects of these backscattered electrons inside the rutile crystal lead to the formation of Kikuchi patterns. The element-resolved Kikuchi patterns of Ti and O differ characteristically, but each can be described fairly well in terms of the dynamical theory of diffraction. Qualitatively, much of the differences can be understood by considering the relative arrangement of the Ti and O atoms with respect to planes defined by the crystal lattice.

1. Introduction

The interaction of electrons with atoms in a crystal is a topic central to condensed matter physics and electron microscopy. For incident electrons, the crystal forms a three-dimensional diffraction grating resulting in complex interference effects. Besides the well-known diffraction patterns of those external electrons that retain their coherence with respect to the incident beam after interaction with a target, one can also observe intensity variations in the angular distribution after incoherent scattering of the impinging electrons. Inside the crystal, these incoherently scattered electrons effectively form internal point sources whose diffraction patterns are referred to as Kikuchi patterns. Kikuchi diffraction effects can be observed in both transmission and reflection geometries [1,2]. Kikuchi patterns are the basis of EBSD (electron backscatter diffraction), a widely used method to characterise the microstructure of materials in the scanning electron microscope (SEM) [3,4].

For large-angle deflections the scattered electron transfers a significant amount of momentum $\boldsymbol{q}$ to a single atom. As a consequence the electron is localised at this atom and the subsequent interference along the outgoing trajectories results in a Kikuchi pattern. For a compound crystal, the electrons can backscatter from different elements at their respective positions in the unit cell. Hence, the Kikuchi pattern will depend on the nature of the backscattering atom. However, in conventional EBSD measurements one generally does not have the knowledge about which atom scattered the electron and the pattern is simply the sum of all contributions.

Recently it has become possible to separate the contributions of electrons scattered from different elements. This was accomplished in a completely different way by two research groups. Saitoh et al. used a scanning transmission electron microscope (STEM) to align a very finely focused electron beam with columns formed by different atoms in a thin sample [5]. For a MgO sample, the observed Kikuchi bands were different when the beam was aligned with either a column of Mg atoms or a column of O atoms.

Winkelmann and Vos [6] used a broad beam, but a large scattering-angle in combination with sub-eV energy resolution. Then the contribution of electrons scattered from O and Al in Al_2O_3 can be separated due to the difference in their recoil energies: $q^2/2M$ with M being the mass of the scattering atom [7].

In a transmission electron microscope (TEM) specific recoil energies are only of the order of phonon energies (compared to ≈ 1 eV in a backscatter geometry as used here), which makes their measurement difficult. However, with the recent demonstration of energy resolution in the phonon range [8], recoil effects should, in principle, be observable in a TEM as well [8,9].

The characteristic Kikuchi features formed by different elements in a crystal structure are due to the different symmetries of the occupied sites in the unit cell. This results in specific atomic configurations with respect to a selected lattice plane $\{h\ k\ l\}$. For instance, for certain $\{h\ k\ l\}$ in a two-element compound like Al_2O_3, atoms of each element can separately be grouped in two layers parallel to $\{h\ k\ l\}$ and then one sees clear differences in the Kikuchi

* Corresponding author.
E-mail address: maarten.vos@anu.edu.au (M. Vos).

http://dx.doi.org/10.1016/j.ultramic.2015.04.018
0304-3991/

pattern of both elements. This observation can be rationalised by the fact that maxima in standing waves of exit probability are aligned with atomic layers of Al in one outgoing direction but with the atomic layers of O for a slightly different outgoing direction [6]. For other lattice planes {*h k l*}, Al and O atoms are mixed in layers parallel to {*h k l*}, and under these conditions the Kikuchi pattern of electrons from either Al or O is thought to be more similar. From this work it became clear that there is a direct relation between the position of the scatterer in the unit cell and the observed intensity variations. Indeed it was subsequently established that for a random positioning of scatterers within the unit cell the Kikuchi contrast should be absent [10]. Here we extend the study to more general directions of a crystal and we investigate to what degree the element-specific Kikuchi patterns differ when the atoms do not form simple rows of either element A or B.

2. Experimental details

The spectrometer was described in detail elsewhere [6,11]. In brief, a 40 keV electron beam impinges on the sample and is analysed using a two-dimensional analyser. The energy resolution of the system is better than 0.5 eV. The analyser accepts electrons whose trajectories are on a segment of a cone with a half-angle of 45°. The incoming beam is along the symmetry axis of this cone. The configuration is sketched in the top panel of Fig. 1. The angle ϕ is determined from the coordinates obtained from the position sensitive detector for each detected electron. A manipulator controls θ_m and is used to point a specific direction towards the analyser.

The scattering angle θ_{scat} of all detected electrons is thus 135°. From the beam spot size (0.2 mm) and the width of the entrance slit in front of the analyser (also 0.2 mm, positioned 130 mm from the sample) one infers an angular resolution for θ_{scat} of $\approx 0.1°$. The ϕ scale of the angular range is calibrated by replacing the entrance slit by a set of apertures, positioned at known distances along the same cone. The φ angular resolution obtained in this way is $\approx 0.1°$. There are angular variations in the detector efficiency. This is compensated by normalising the measured angular distribution with that obtained for a polycrystalline film which has no Kikuchi contrast for a broad beam.

We chose a single crystal of rutile (TiO_2) as a target. The {1 1 0} surface was sputtered in vacuum with 2 keV Ar^+ ions, and annealed subsequently such that a mild red glow of the crystal was observed. The annealing restored the stoichiometry of the surface layer and a low-energy electron diffraction (LEED) pattern was visible which was used to determine the crystal orientation. Using this information the sample was roughly rotated such that a major zone axis (here [1 0 0], [1 1 0] or [1 1 1]) was facing the analyser. By varying the rotation angle θ_m by a few degrees, the specific angular orientation with a strong peak in the Kikuchi band was used to determine the crystal orientation more precisely. The angular resolution of the manipulator (θ_m) is $\approx 0.2°$ and such a resolution is required as the pattern can change appreciably over 0.2°. The absolute minimum sample size is 0.5 mm, dictated by the beam diameter (0.2 mm), but in practice the sample size of ≈ 3 mm is the lower limit, as the point where the beam intersects the sample changes with θ_m rotation for our manipulator.

The spectra shown in Fig. 1 are taken for a thermally grown polycrystalline film and for a single crystal of TiO_2 positioned in two different orientations (to be discussed later). There are two elastic peaks in this spectrum. The intensity between 0 and 3 eV was attributed to electrons scattered from Ti and between 3 and 6 eV to electrons scattered from O. The separation of the peaks is indistinguishable from what is calculated for 40 keV electrons scattering over 135° from (free) O and Ti atoms. A very minor

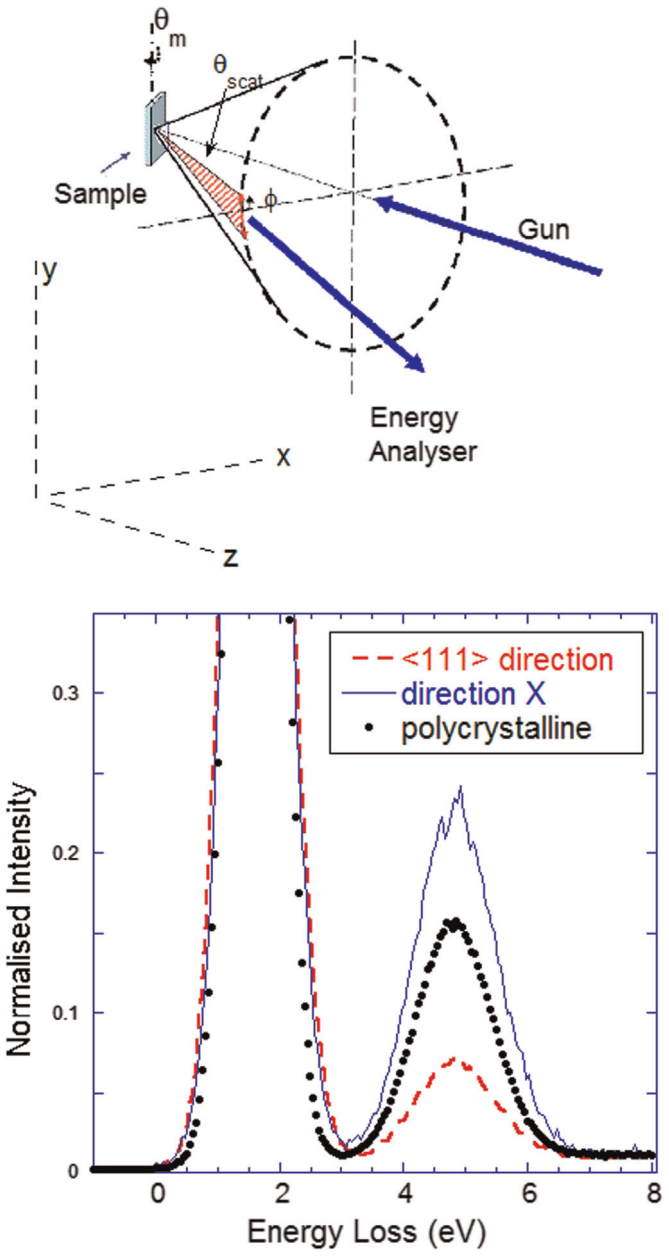

Fig. 1. The left panel shows a sketch of the experimental configuration as well as the coordinate system used. The right panel shows three spectra of TiO_2, with the Ti elastic peak areas normalised to unit area. The second peak neat 5 eV energy loss is attributed to electrons scattered from O atoms. One spectrum was taken with the analyser along ⟨1 1 1⟩, one with the analyser positioned along a direction marked X in Fig. 7 and one spectrum for a thermally grown polycrystalline film.

background is present under the O peak, but this background does not affect the outcome of the experiment at the level discussed here. For the polycrystalline film there is good agreement between the calculated intensity of the Ti and O elastic peaks, but obviously there is a large variation possible for the Ti:O peak intensity ratio for TiO_2 single crystals. This is a clear indication that diffraction effects can modify the observed Ti and O elastic peak intensities in a very significant way and these variations are the subject of this paper.

3. Theoretical analysis

Kikuchi patterns can be simulated by using a Bloch wave approach to the dynamical theory of electron diffraction [12]. In the

absence of energy filtering, the calculated EBSD intensity distribution of a compound crystal like TiO_2 is the weighted sum of the distribution calculated for electrons scattered from Ti or from O. The weighting coefficients for the contributions of Ti and O are based on the ratio of the differential elastic scattering cross section of O and Ti as well as on the stoichiometry. Here we assume that this cross section scales with Z^2, like in the Rutherford cross section for elastic scattering.

We applied the Bloch wave approach for the calculation of the angle-dependent intensities of backscattered electrons. Rutile has a tetragonal structure with $a=b=4.584$ Å, $c=2.953$ Å, space group $P\,4_2/m\,2_1/n\,2/m$ (International Tables for Crystallography, No. 136 [13]), point group 4/mmm. In the TiO_2 simulations, 1534 reciprocal lattice points hkl (reflectors) with a minimum distance $d_{hkl} > 0.040$ nm and an intensity larger than 7% relative to the strongest reflector intensity (square of the absolute value of the structure factor) have been taken into account. In the Debye–Waller factor a mean square displacement of 0.0001 nm^2 was used to consider thermal vibrations of both Ti an O. According to the TPP2-formula [14] the inelastic mean free path is 45 nm for 40 kV electrons. As no inelastic energy loss should occur along the incoming or outgoing trajectory for an event to contribute to the elastic peak, the mean outgoing trajectory length will be of the order of 22 nm [15]. When calculating the Kikuchi pattern for an outgoing trajectory length of 22 nm we find that the theory overestimates the contrast significantly. Better agreement with the experiment was obtained using values near 10 nm for the average length of the outgoing trajectory, and this value was adopted here. The theory was always compared directly to the experiment, i.e. the calculated results were *not* convoluted by the experimental angular resolution.

As an introduction to the following element-resolved Kikuchi features, we first show a Kikuchi pattern as is measured in a conventional EBSD setup using a phosphor screen and we compare it to a simulated pattern in Fig. 2. In this EBSD measurement, the incoming energy was 18 keV. Overall the agreement between the experimental and calculated pattern is good, as judged visually and by the normalized cross-correlation coefficient of $r=0.67$ between the experimental and the simulated pattern [16,17]. For better orientation, in the simulated pattern, we marked the two regions where we measured the element-resolved Kikuchi band profiles as shown in Figs. 6 and 7.

We show in Fig. 3 the element-resolved contributions to the simulated EBSD data as in Fig. 2. This separation for different elements is easily done in a calculation as the total EBSD pattern is the sum (weighted by the Rutherford cross section) of the pattern originating from O atoms and the pattern originating from Ti atoms. The characteristic differences between the contributions of Ti and O to the EBSD pattern are obvious. The average contribution of O is about 0.26 of that of Ti, as estimated from the Z^2-dependence of the Rutherford cross section. Due to the diffraction effects, there are regions in the EBSD pattern, where the O/Ti ratio goes up to approximately 40–50%, as can be seen in Fig. 3(c). In this figure, the dark bands show the Kikuchi bands which are dominated almost solely by the Ti contribution. While some higher-intensity bands show an increased O contribution, the intensity is never dominated by O, which would result in O/Ti values greater than 1.0.

Electrons with a comparatively broad energy spectrum up to several hundred eV near the incident beam energy can contribute to the visible diffraction effects in a conventional EBSD pattern [15,18]. In contrast, in our electrostatic spectrometer we measure the energy with sub-eV resolution. The price one has to pay for the improved energy resolution, this is an enormous drop in data acquisition rate. It is thus not feasible with our spectrometer to acquire a fully two-dimensional map of the Kikuchi pattern. We

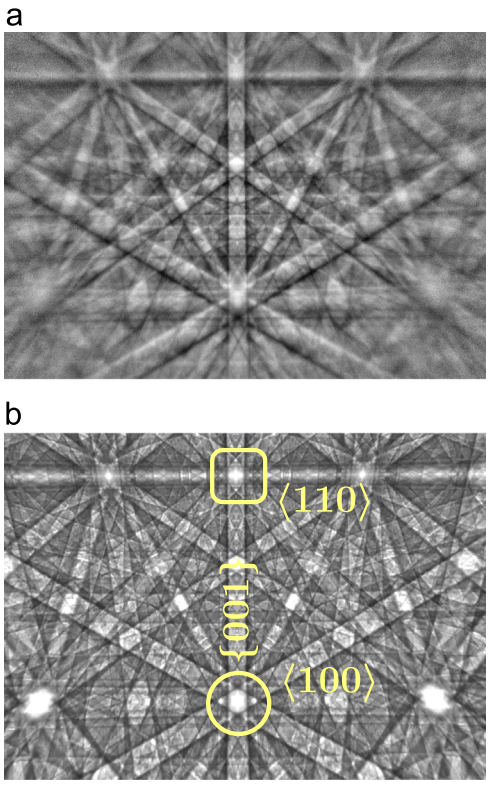

Fig. 2. Experimental rutile EBSD pattern and dynamical simulation. The marked areas correspond to the zone axis regions which were investigated in the spectroscopic measurements in Fig. 6 (circle around ⟨1 0 0⟩) and Fig. 7 (rectangle around ⟨1 1 0⟩): (a) rutile, experimental EBSD pattern, $E_0=18$ kV and (b) rutile, simulated EBSD pattern, normalized cross correlation with experiment r=0.67.

carried out our measurements only along specific 1D-lines in the overall 2D intensity distribution. To avoid getting completely lost in the intricate structures seen in the measurement we first discuss the calculated Kikuchi pattern for Ti and O, highlighting the differences for both elements and explaining these differences in qualitative terms. Then we test the validity of the calculations by comparing them along specific line segments with the experiment.

In order to characterize the Kikuchi signal distribution only the fundamental sector of the point group 4/mmm needs to be considered. It is defined by [1 0 0], [1 1 0] and [0 0 1]. The two octants in Fig. 4 are equivalent but display the stereographic projection of the signals of electrons scattered from Ti and O respectively. Although there are some similarities, overall the patterns are very different. We can group the crystal planes in four categories, depending on the appearance of their Kikuchi bands:

Type A planes: Planes that form fairly similar Kikuchi bands for both O and Ti. Examples here are the {0 0 1} and {0 3 1} planes.

Type B planes: Planes where the O Kikuchi bands have a peculiar shape, a strong minimum surrounded by shoulders of significant intensity. The corresponding Ti Kikuchi lines have a width that is approximately equal to the width in the minimum of the O Kikuchi bands. This is the case for the {0 1 1} and {0 1 0} planes.

Type C planes: Planes that have pronounced Kikuchi bands for O, but very weak bands for Ti. Examples here are the {1 1 1} planes, which have distinct Kikuchi bands for O, but only very faint bands for Ti.

Type D planes: For these planes the reverse is true for e.g. {1 2 1} planes, which have well developed Ti Kikuchi bands but virtually no bands for O.

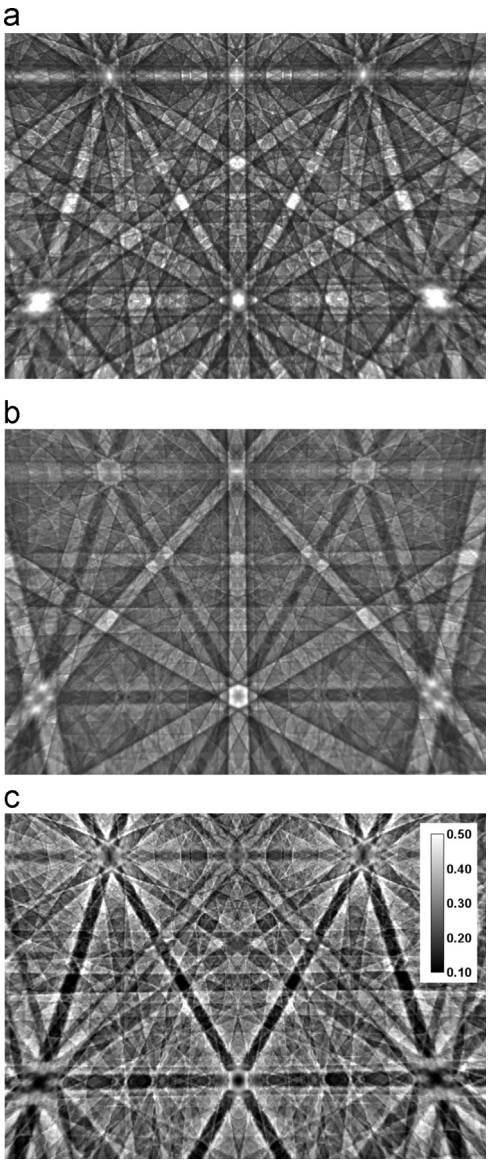

Fig. 3. Element-resolved analysis of the simulated rutile EBSD data as shown in Fig. 2: (a) Ti contribution; (b) O contribution $\times 3$; and (c) ratio of O to Ti contribution.

For understanding EBSD Kikuchi patterns within the dynamical theory of diffraction it is easiest to consider the problem using time reversal symmetry: the chance that an energetic electron, which has scattered incoherently from a nucleus, leaves the crystal in a specific direction is proportional to the chance that an electron impinging on the crystal from that direction scatters from that nucleus.

An impinging electron travelling near Bragg conditions will interact with the crystal and standing waves will form. The maxima (minima) in the probability density associated with these standing waves can coincide with an atomic position, causing maxima (minima) in the observed Kikuchi pattern [19]. In Fig. 5 we draw the atomic configuration of the planes to understand their interaction with the standing waves.

Let us start with the {0 0 1} as type A plane (Fig. 5(a)). There are two different layers of atoms parallel to {0 0 1}. They are not equivalent, but each of the two layers contains both O and Ti atoms. If the maxima in the standing wave of exit probability coincide with either of these layers, then it will affect the Ti and O intensities in the same way. Thus for {0 0 1} we expect a similar diffraction signal for O and Ti.

The {0 1 1} is an example of a type B plane and the layers of atoms are completely different (Fig. 5(b)). They consist either of only Ti atoms or of only O atoms. Thus if the maximum of the standing waves coincides with the layer containing Ti atoms, then the backscattering probability from O atoms will have a minimum. If the beam direction is changed in such a way that the sign of the excitation error changes then the position of the maxima will move away from the Ti layer and be closer to the pair of layers that contain the O atoms [20]. This explains the minima in the {0 1 1} O Kikuchi patterns right at the crystal plane direction and maxima slightly away from it, as can be seen in Fig. 4. The situation is almost identical for {0 1 0} (Fig. 5(b)) and indeed the O Kikuchi pattern for the {0 1 0} resembles the {0 1 1} in Fig. 4.

Now let us consider {1 1 0} (Fig. 5(a)) which represents an intermediate case. The layers parallel to {1 1 0} through Ti atoms contain also O atoms, but there are additional layers made of only O atoms. Here we expect Ti atoms to have a well defined maximum, when the standing wave coincides with the Ti containing layers, but a less pronounced behaviour for the O atoms, as always some of the O atoms are near the maxima and minima of the standing waves.

The {1 1 1} planes are strong for scattering from O and weak for scattering from Ti and are thus clear examples of type C planes.

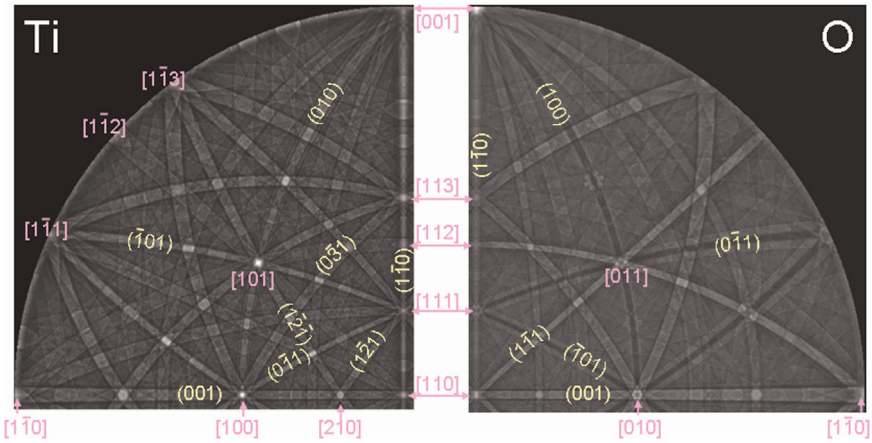

Fig. 4. The stereographic projection (centred on [1 1 0]||(1 1 0)) of the calculated Kikuchi patterns, separated for the Ti (left half) and O (right half) contribution for a (1 1 0)-rutile. The energy was 40 keV. Several lattice directions [*u v w*] and planes (*h k l*), mentioned in the main text, are indicated for convenience.

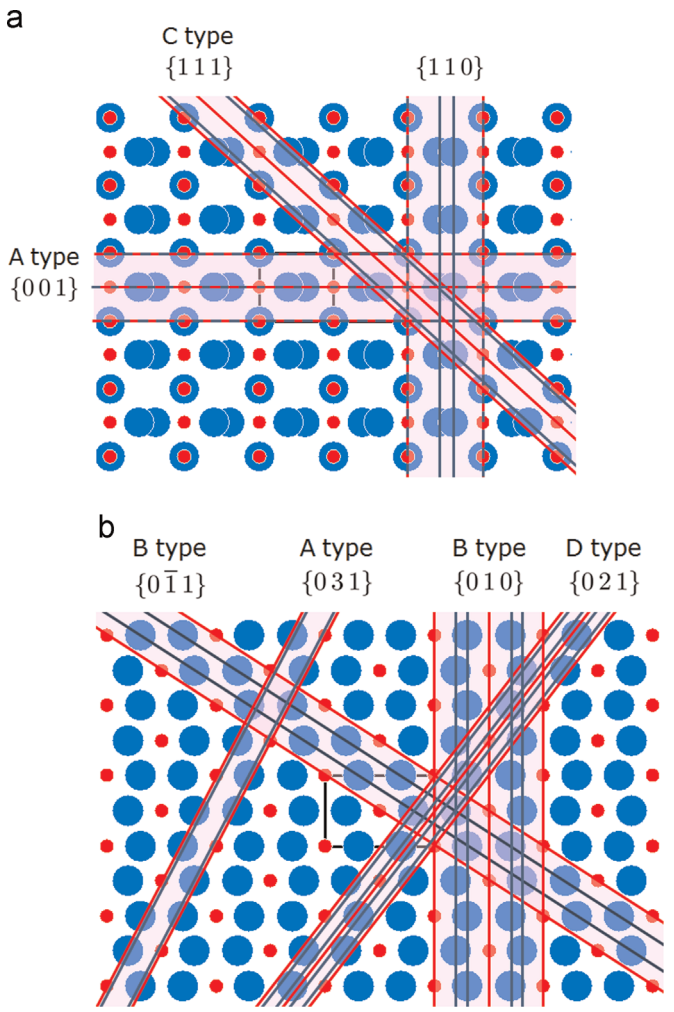

Fig. 5. Arrangement of atom layers parallel to some horizontally aligned lattice planes {*h k l*} in rutile. Ti is coloured in red, O is drawn in light blue. The unit cell is given as a wire frame: (a) projection along ⟨1 1̄ 0⟩ and (b) projection along ⟨1 0 0⟩. (For interpretation of the references to color in this figure caption, the reader is referred to the web version of this paper.)

There is one layer parallel to {1 1 1} containing only Ti atoms, and another layer containing both Ti and O atoms, some of the O atoms slightly moved below or above the layer (Fig. 5(a)). If the maxima in the standing wave are aligned with the latter layer the O intensity will be increased, but the Ti intensity will be much less affected, as an equal number of Ti atoms are near the minima.

The reverse is found for {1 2 1} which is an example of a type D plane. Here the Ti atoms line up nicely in layers, but the O atoms are more uniformly dispersed over several layers. As a consequence the Ti {1 2 1} Kikuchi bands are clearly visible but the O ones are not (see Fig. 4).

Finally we show the {0 2 1} and {0 3 1} in Fig. 5(b). Parallel to {0 2 1} no clear layers are definable since the atoms are quite evenly distributed between the lattice planes. For this case the Kikuchi pattern of both Ti and O are expected to be relatively weak as is confirmed by the calculation as shown in Fig. 4. In contrast, for the {0 3 1} case the Ti and O atoms line up nearly perfectly in horizontal layers parallel to {0 1 3} (the O atoms slightly buckled below and above the layers defined by the Ti atoms). Indeed Ti and O show well-developed, nearly identical Kikuchi bands (type A plane).

In the above we described the diffraction effects of the crystal in the two-beam case: only one reflected Bragg beam is excited and this causes the formation of a simple sine- or cosine-like standing wave. Especially near the zone axes, however, more than one Bragg beam will usually be excited. Qualitatively it appears that the intensity here can be seen in a first approximation as the sum of the planar diffraction contribution, e.g. if two planes cross that show enhancement of intensity, then the zone axis direction will show an even larger enhancement of intensity. The zone axis fine structure, however, is influenced by many-beam effects which do not lead to a simple addition of intensities but to complex interference effects.

4. Experimental results

The measurements near the ⟨1 0 0⟩ zone axis direction are shown in Fig. 6. Also shown in this figure is the theory near this direction, plotted *not* as a stereographic projection but in the coordinate system of the experiment (see Fig. 1, left panel) where θ refers to the sample rotation axis, relative to the major zone axis direction, and ϕ is the angle of the detected electron relative to centre of the main (horizontal) Kikuchi band. Note that the actual change in direction if ϕ changes by x is approximately $x \sin \theta_{scat}$ with $\theta_{scat} = 135°$. Measurements were done at the ⟨1 0 0⟩ zone axis and 4° and 8° away from this direction. The rotation axis was the normal of {0 0 1}, i.e. the {0 0 1} plane was always pointing towards the analyser. However, a comparison with the theory showed that significant better agreement was obtained (especially for the scans away from ⟨1 0 0⟩) if we assume that these measurements had been performed at 0.2°, 4.2° and 8.2°. These angles were used for the detailed comparison with theory.

In these and all subsequent plots of angular distributions the bottom of the graph corresponds to zero intensity for both the experiment and the theory. In the zone axis direction itself the Ti and O Kikuchi patterns are different. Ti has a maximum intensity at the exact ⟨1 0 0⟩ direction, whereas O has a local minimum. The ⟨1 0 0⟩ zone axis is formed by the intersection of five prominent lattice planes, three of them have a minimum for O in the exact plane direction. The local minimum at the zone axis direction for O reflects that, and this is seen in both experiment and calculation. For the angular distributions at θ=4.2° and θ=8.2° away from ⟨1 0 0⟩ zone axis the {0 0 1} Kikuchi band (centred at ϕ=0°) is remarkably similar for Ti and O, even the details of the shape of this Kikuchi band are very similar for both Ti and O, in both experiment and calculation, as expected for a type A plane.

For the measurement at θ=4.2° there is a strong maximum at ϕ=4° in the Ti angular distribution which is absent in the O angular distribution. For θ=8.2° the beginning of a strong feature is visible at the edge of the Ti angular distributions measured ($\phi \approx 6.5°$), which is again absent in the O angular distribution. This is due to the strong central Kikuchi bands for Ti {0 1 1} (type B planes) that are absent for the O {0 1 1} planes.

Next we study directions close to the surface normal which parallel to ⟨1 1 0⟩. Again the {0 0 1} Kikuchi band was covered by the angular range of the analyser. Results are shown in Fig. 7. The zone axis direction has now a maximum intensity for both Ti and O. Moving away from the zone axis ⟨1 1 0⟩ we see additional peaks in the O intensity distribution, moving to higher ϕ values with increasing θ (e.g. the peak near $|\phi| = 3°$ in the angular distribution measured for θ=2°). This is the {1 1 1} (a type C plane) that stands out for O but is very weak for Ti.

Close to the zone axis ⟨1 1 0⟩ the angular distributions are affected by the entire zone, i.e. by all lattice planes {*h* $\bar{h}$ *l*}. The shape of the {0 0 1} Kikuchi band profile is as a consequence rather different for Ti and O, it is only at θ=5° that the shape of the O (0 0 1) Kikuchi band starts approaching that of the Ti (1 0 0) band. In the Ti Kikuchi pattern there appears to be a diamond shaped area around the ⟨1 1 0⟩ zone axis with increased intensity. The

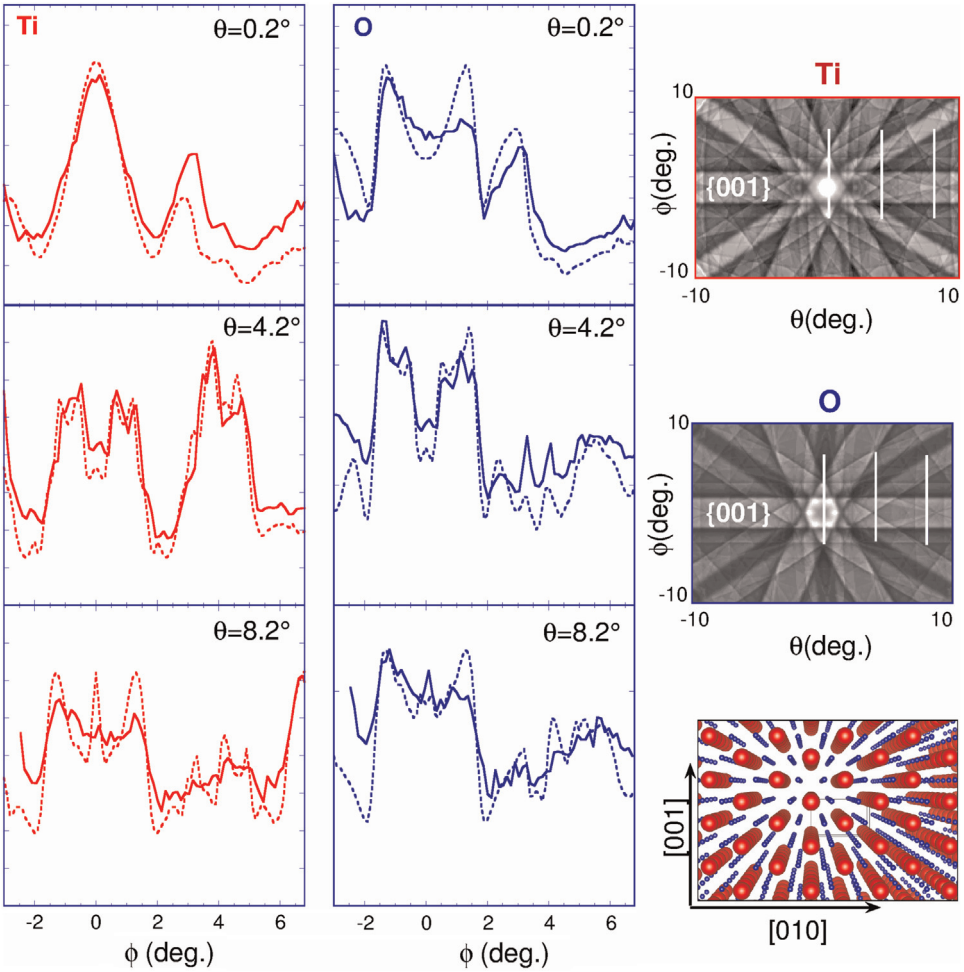

Fig. 6. Element-specific measured (full line) and calculated {1 0 0} band profiles (dashed line) for different angular distances to ⟨1 0 0⟩. The left panel displays the scattered electron signal from Ti whereas the central panel reflects the O signal. The zone axis direction corresponds to $\theta=0$, $\phi=0$. On the right the simulated Kikuchi patterns around ⟨1 0 0⟩ are shown, for electrons scattered from Ti (top) and O (middle). The slices along the intensity was measured are indicated by thick lines in these grey-scale plots. The lower panel is a view of the rutile crystal along ⟨1 0 0⟩ in the same orientation as the greyscale plots. (larger (red) spheres: Ti atoms, smaller (blue) spheres: O atoms. (For interpretation of the references to color in this figure caption, the reader is referred to the web version of this paper.)

measurement at $\theta=2°$ intersects a corner of this diamond-shaped area with enhanced intensity. As a consequence Ti displays a very sharp peak there in its angular distribution at $\phi=0$. The diamond shaped features are caused by many-beam interference of lattice planes belonging to the {1 1 0} zone. For $\theta=5.5°$ the Ti intensity within the {1 0 0} Kikuchi band is rather weak, whereas the O {1 0 0} Kikuchi band is well developed. In this region the Ti:O signal strength is one of the lowest, and the O-rich spectrum of Fig. 1 was acquired in the region marked *X*.

In Fig. 8 we compare the angular distributions for three major directions: ⟨1 0 0⟩ (same angular distribution as in Fig. 6), ⟨1 1 0⟩ (measurement with the crystal rotated by 90° around the sample normal, i.e. the line measured now is indicated by a dashed line in the grey-scale panels of Fig. 7.) and ⟨1 1 1⟩.

In all cases the Ti angular distribution displays a 'normal behaviour', i.e. showing a pronounced peak in the zone axis direction. There is a clear change in shape of the angular distribution before and after rotation over 90° for the scan through the ⟨1 1 0⟩ zone axis (Fig. 7, left panel with $\theta=0$ and Fig. 8, 'through ⟨1 1 0⟩'). After rotation the angular distribution shows two secondary peaks (at $\phi=\pm 3°$). These are the same directions as the sharp peak in the angular distribution in $\theta=2$ of Fig. 7 i.e. the secondary peaks correspond to the corners of the diamond shape area mentioned before.

More interesting is the behaviour of the O angular distribution. Only for the ⟨1 1 0⟩ direction the O angular distribution has a maximum in the zone axis direction. For the ⟨1 0 0⟩ angular distribution the O distribution shows a local minimum as discussed before. Surprisingly, for the ⟨1 1 1⟩ direction the O angular distribution does not show a pronounced peak near the zone axis direction at all, with the maxima in the observed intensity distribution well away from the zone axis direction. The ⟨1 1 1⟩ direction can be seen as the intersection of different planes. Of these planes only the (1 1 0) plane shows a relatively weak Kikuchi band for O. Two {1 0 1}-type planes are of type B, and do not contribute for O to a peak. In addition two {1 2 1}-type planes intersect the ⟨1 1 1⟩ zone axis. These are type D planes contributing to enhanced intensity Ti peak, but show little or no intensity for the O peak. As a consequence the O-derived intensity distribution shows virtually no peak near ⟨1 1 1⟩, whereas the Ti signal is strongly peaked.

5. Discussion and conclusion

The Kikuchi profiles of O and Ti in rutile were compared. Sometimes the Kikuchi profiles of Ti and O are very different, sometimes rather similar. If and how the Ti and O Kikuchi bands are different can be understood quite accurately by considering

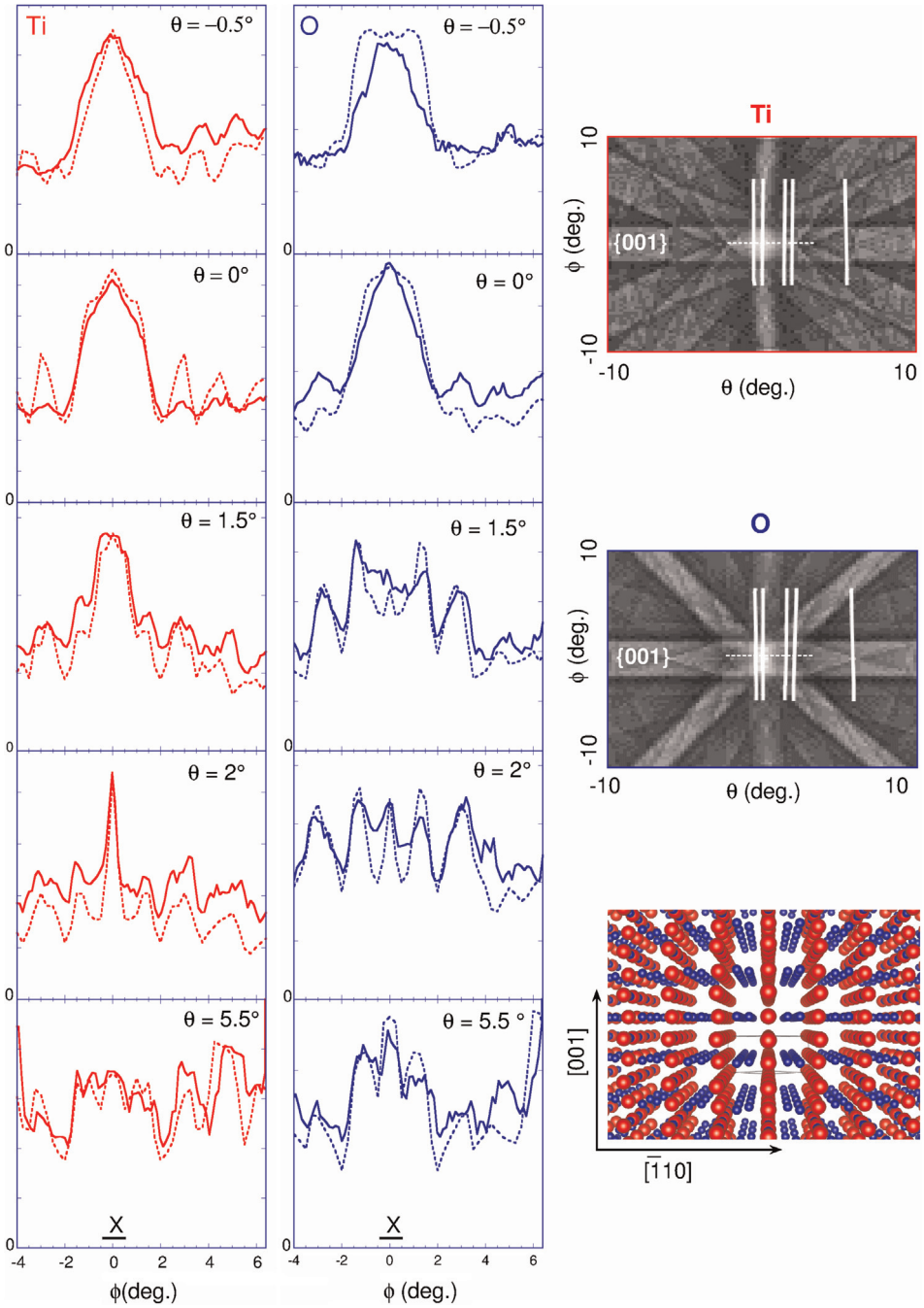

Fig. 7. Same as Fig. 6 but now for the ⟨1 1 0⟩ zone axis. The (horizontal) dashed line in the grey scale plots refers to the measurement of Fig. 8, centre panel. In the lowest panels, "x" is the direction where the energy spectrum of Fig. 1 was measured.

the atomic arrangement of the atoms in the plane.

Many features seen in the theory are reproduced in the experiment. A fully quantitative comparison reveals also many differences. This is in part due to shortcomings in the spectrometer. The detector response is not uniform and this is corrected for by measuring the intensity of a polycrystalline or amorphous sample as well, where we do not expect angular variations of the intensity. The detector response depends also somewhat on the sample position, and hence there are limits to the accuracy of this correction method. Another cause of error is the accuracy by which the sample rotation (θ_m) is controlled.

The theoretical results depend on the number of beams considered. The main features are well reproduced using a limited number of diffracted beam but details, especially away from the main crystallographic directions, change when more beams are included. However these changes do not affect the level of agreement between experiment and theory much. Another factor that determines the level of agreement between theory and experiment is the sample quality and alignment accuracy. Sputter cleaning results in a preferential removal of O from the surface. The stoichiometry will be restored by the anneal treatment afterwards as can be seen by the absence of a characteristic loss feature, associated with Ti^{3+} in the reflection electron energy loss spectrum taken at lower incoming energies. When perfected, the experiments described here should be a good tool to study the order in the oxygen sub-lattice several 10 s of nm below the surface. Another parameter that is related with the order in the O sub-lattice is the mean vibrational amplitude of these ions. The Ti

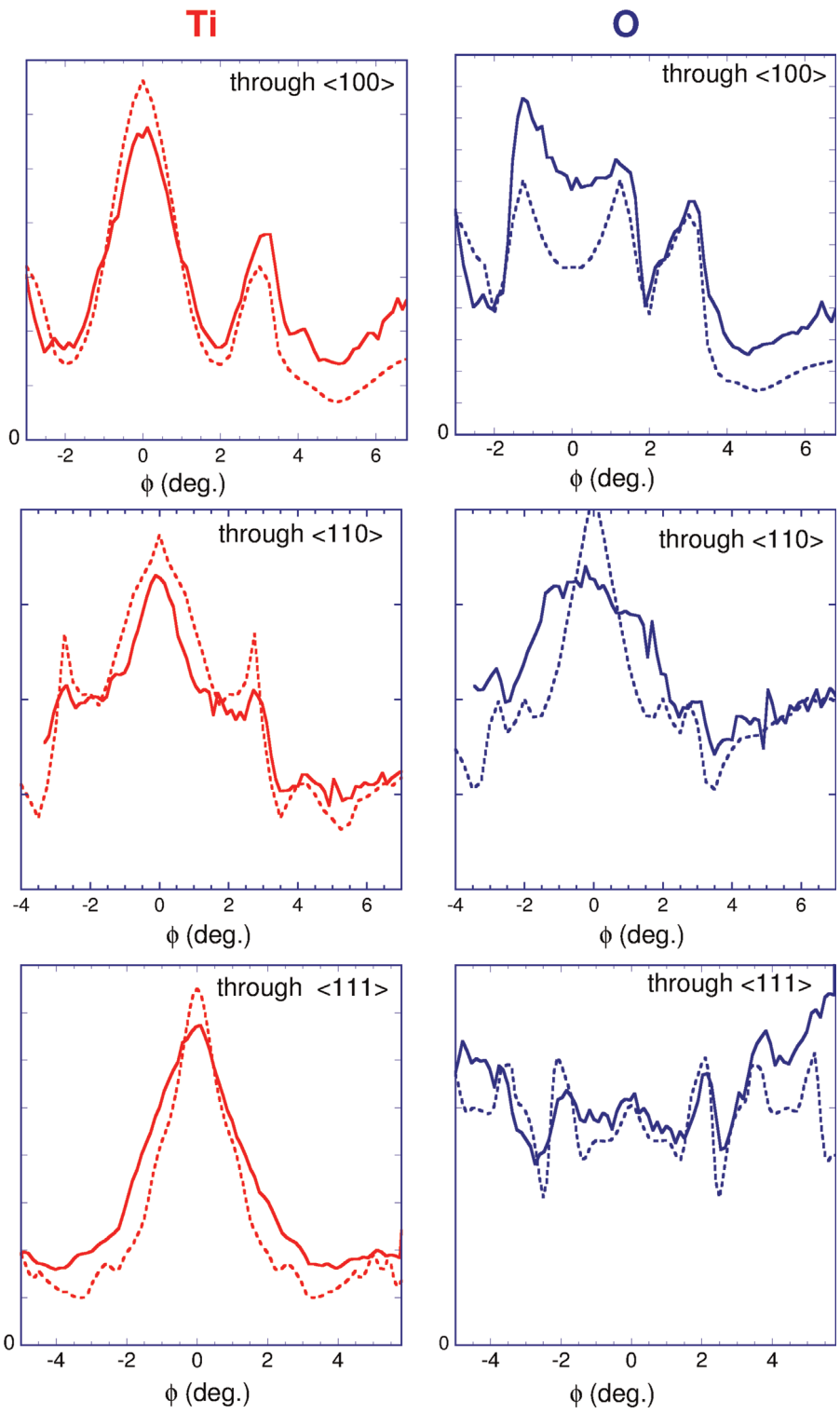

Fig. 8. The Kikuchi profiles of O and Ti through the three main crystallographic directions.

and O vibrational amplitudes are currently modelled in a simple Einstein model.

From a theoretical point-of-view these experiments are a test of the dynamical theory of diffraction. The energetic electrons are described by standing waves. The signal is proportional to the electron density at the atomic sites i.e. if the atom is near a maximum or a minimum in the probability density of these standing waves. By separating the signal from O and Ti we can determine this overlap at the O and Ti sites separately, and hence resolving more features of the density of the probing electron in the crystal.

Maybe the most interesting result from this work is that the differences between the O and Ti Kikuchi patterns can be straightforwardly rationalised by considering the atomic configuration of various planes. This observation makes it attractive to consider how, from the measurement of an element-specific Kikuchi pattern, one can get information about the crystallographic structure near the surface. The first such measurement is already under way,

where we try to determine the substitutional fraction of Au atoms in Au-implanted, laser-annealed Si crystals based on their Kikuchi patterns.

Acknowledgements

This research was made possible by funding of the Australian Research Council.

References

[1] S. Nishikawa, S. Kikuchi, Proc. Imp. Acad. 4 (1928) 475.
[2] S. Kikuchi, Proc. Imp. Acad. 4 (1928) 354.
[3] A.J. Schwartz, M. Kumar, B.L. Adams (Eds.), Electron Backscatter Diffraction in Materials Science, 1st ed.,Kluver Academic, Plenum Publishers, New York, Boston, Dordrech, London, Moscow, Netherlands, 2000, p. 350.
[4] A.J. Schwartz, M. Kumar, B.L. Adams, D.P. Field (Eds.), Electron Backscatter Diffraction in Materials Science, Springer Science+Business Media, New York, NY, 2009.
[5] K. Saitoh, Y. Tatara, N. Tanaka, J. Electron Microsc. 59 (2010) 387.
[6] A. Winkelmann, M. Vos, Phys. Rev. Lett. 106 (2011) 085503.
[7] M. Vos, Phys. Rev. A 65 (2001) 12703.
[8] O.L. Krivanek, T.C. Lovejoy, N. Dellby, T. Aoki, R.W. Carpenter, P. Rez, E. Soignard, J. Zhu, P.E. Batson, M.J. Lagos, R.F. Egerton, P.A. Crozier, Nature 514 (2014) 209.
[9] G. Argentero, C. Mangler, J. Kotakoski, F. Eder, J. Meyer, Ultramicroscopy 151 (2015) 23.
[10] A. Winkelmann, M. Vos, Ultramicroscopy 125 (2013) 66.
[11] M. Vos, M. Went, A. Winkelmann, Ultramicroscopy 109 (2009) 1211.
[12] A. Winkelmann, C. Trager-Cowan, F. Sweeney, A.P. Day, P. Parbrook, Ultramicroscopy 107 (2007) 414.
[13] T. Hahn (Ed.), International Tables for Crystallography. Vol. A: Space-group Symmetry, 4th ed.,Kluver Academic Publishers, Dordrecht, Boston, London, 1995.
[14] S. Tanuma, C. Powell, D. Penn, Surf. Interface Anal. 17 (1991) 911.
[15] A. Winkelmann, K. Aizel, M. Vos, New J. Phys. 12 (2010) 053001.
[16] R.C. Gonzalez, R.E. Woods, Digital Image Processing, Prentice-Hall, Upper Saddle River, NJ, 2002.
[17] X. Tao, A. Eades, Microsc. Microanal. 11 (2005) 341.
[18] A. Deal, T. Hooghan, A. Eades, Ultramicroscopy 108 (2008) 116.
[19] A. Winkelmann, in: A.J. Schwartz, M. Kumar, B.L. Adams, D.P. Field (Eds.), Electron Backscatter Diffraction in Materials Science, Springer, Berlin, 2009, Chapter 2.
[20] C.J. Humphreys, Rep. Prog. Phys. 42 (1979) 1825–1887.